



Homogeneous and flexible mullite nanofibers fabricated by electrospinning through diphasic mullite sol–gel route

Xiaolei Song¹, Yunzhu Ma^{1,*}, Juan Wang¹, Bing Liu¹, Shuwei Yao¹, Qingshan Cai^{1,*}, and Wensheng Liu^{1,*}

¹ State Key Laboratory of Powder Metallurgy, Central South University, Changsha 410083, China

Received: 20 April 2018

Accepted: 4 July 2018

Published online:
13 July 2018

© Springer Science+Business
Media, LLC, part of Springer
Nature 2018

ABSTRACT

In the present work, homogeneous and flexible mullite nanofibers were successfully prepared by electrospinning method through the conventional diphasic mullite sol–gel route for the first time. Alumina sol prepared using aluminum acetate (stabilized with boric acid) was mixed with colloidal silica to prepare the precursor mullite sol. Polyvinyl pyrrolidone (PVP) was applied as polymer additive. General rules for preparing desired as-spun nanofibers and fiber morphological evolution were discussed, and elemental analyses and mechanical properties of mullite nanofibers were studied. It was found that uniform as-spun nanofibers were obtained when the mass ratio of PVP solution to precursor sol was 1.5. Upon calcining, $\text{Al}_4\text{B}_2\text{O}_9$ and $\text{Al}_{18}\text{B}_4\text{O}_{33}$ phase formed instead of $\gamma\text{-Al}_2\text{O}_3$ due to the introduction of boron. Average fiber diameter decreased unceasingly with the calcination temperatures increased from 800 to 1200 °C because of the densification related to the phase transformation and the presented amorphous SiO_2 . After calcining at 1000 °C, relatively smooth fiber surface was obtained owing to the self-repairing ability for surface defects. Mullite nanofibers with preferable morphology possessed Al/Si molar ratio of 2.98, homogeneous elemental distribution, elastic modulus of 25.18 ± 1.29 GPa and outstanding flexibility.

Introduction

As one of the most important ceramic materials, mullite ($3\text{Al}_2\text{O}_3 \cdot 2\text{SiO}_2$) fibers are famous due to the outstanding dielectric properties, superior chemical stability, low thermal conductivity and excellent high-temperature properties [1–3]. They have been found extensive applications in areas of insulation,

filtration and catalyst, or been used as reinforcement for ceramics, metals and resins in the past several decades [4–6]. In recent years, with the rapid development of nanomaterials science, ceramic nanofibers, owing to the ultralow thermal conductivity, superior flexibility and ultrahigh mechanical properties, have been used to prepare insulating materials and draw intensive attention. Si et al. [7] fabricated an

Address correspondence to E-mail: zhuzipm@csu.edu.cn; caiqingshan@csu.edu.cn; liuwensheng@csu.edu.cn

ultralight, highly compressible and resilient nanofibrous ceramics using silica nanofibers as one of the starting materials. The product exhibited an ultralow thermal conductivity due to the extremely high porosity generated by the use of the nanofibers. Wang et al. [8] also synthesized multifunctional ceramic nanofiber sponges successfully using a variety of oxide ceramic nanofibers, including TiO₂ nanofibers, ZrO₂ nanofibers, yttria-stabilized ZrO₂ nanofibers and BaTiO₃ nanofibers. Apparently, mullite nanofibers, which have better thermal and mechanical properties than those ceramic nanofibers theoretically, are promising materials to prepare nanofibrous ceramics used in insulation area. Therefore, it is meaningful to prepare lightweight and flexible mullite nanofibers with excellent structural stability under high temperature.

To fabricate ceramic fibers in nanoscale, electrospinning is one of the most promising techniques [9]. Undoubtedly, mullite nanofibers have been successfully fabricated by electrospinning [10–12]. When fabricating electrospun mullite nanofibers, a major step is to prepare mullite precursor sol. As we know, mullite precursor sol can be divided into monophasic sol and diphasic sol according to the homogeneity degree of the aluminum and silicon [13]. Monophasic sol forms when aluminum and silicon are mixed at atomic level, and diphasic sol generates when the homogeneity scale of aluminum and silicon is between 1 and 100 nm. Most commercial mullite fibers are produced through the diphasic sol–gel route, such as Nextel™ 312, 440 and 550 ceramic fibers from 3 M Company [3, 14, 15]. A main reason for this is that the mullite formation temperatures of the diphasic gels (> 1200 °C) are much higher than that of the monophasic gels (< 1000 °C) [13], which means that the diphasic gel-derived mullite fibers have more stable structure and mechanical properties while applied under high-temperature circumstance. However, most electrospun mullite nanofibers were prepared by the monophasic sol–gel route according to their raw materials and preparation processes. Wu et al. [10] selected hydrous aluminum nitrate (AN), aluminum isopropoxide (AIP) and tetraethoxysilane (TEOS) as the starting materials. The precursor sol was prepared when aluminum and silicon hydrolyzed simultaneously. This was a typical synthetic route of the monophasic sol. It was found that the mullite nanofibers were nonuniform with large grain sizes after calcining at 1200 °C. Mohammad et al.

[11, 16] fabricated electrospun mullite fibers using AN, AIP and TEOS as raw materials as well, and their fiber products were not uniform and could not retain a stable structure under high-temperature circumstance. Other researches normally selected AN–AIP–TEOS system and similar preparing processes to prepare mullite nanofibers [17–19]. Dong et al. [20] fabricated electrospun mullite nanofibers derived from diphasic sol for the first time. Mullite phase formed at 1200 °C for their fiber product, and a grain size of approx. 100 nm was obtained after calcining at 1500 °C, which was much smaller than that of electrospun mullite nanofibers derived from monophasic sol. Aluminum tri-sec-butoxide and polymethylsiloxane, as two novel raw materials, were used as the sources of alumina and silica. When preparing the diphasic sol, dibutyltin dilaurate was used as the cross-linking catalyst and a mixture of isopropanol and ethylacetate was used as the solvent. The common and low-cost route to fabricate diphasic mullite sol is mixing alumina sol and silica sol together. Obviously, the mullite precursor sol in Dong's study was not prepared through the conventional diphasic sol synthetic route. Considering that their preparation process was a bit complex and the produce cost was relatively high, making efforts to synthesize electrospun mullite nanofibers using the conventional diphasic mullite sol was meaningful.

Based on the above discussion, the present work aimed to prepare homogeneous and flexible electrospun mullite nanofibers through the conventional diphasic mullite sol–gel route and explore general rules for preparing spinning solution, electrospinning and fiber morphological evolution. Aluminum acetate stabilized with boric acid was used to prepare the alumina sol. Commercial colloidal silica was used as the silica source. Polyvinyl pyrrolidone (PVP) was used as the spinning additive. It should be noted that the introduction of boron could lower the formation temperature of mullite phase [2, 21], but it would not affect the feasibility of preparing diphasic mullite nanofibers theoretically. Besides, the introduced boron could exert beneficial influences on the properties of mullite fibers. Specifically, it contributed to improve the flexibility and decrease the density effectively, and would widen their applications actually [2, 21]. To produce uniform as-spun nanofibers, spinning solutions with different mass ratios of PVP solution to precursor sol were prepared. The morphology and chemical structure of as-spun

nanofibers, the microstructure evolution of diphasic mullite nanofibers during calcination, and the elemental analyses and mechanical properties of the nanofiber product were investigated in detail.

Experimental procedure

Materials

Aluminum acetate stabilized with boric acid ($\text{Al}(\text{OH})_2(\text{OOCCH}_3)\cdot 1/3\text{H}_3\text{BO}_3$) was supplied by Strem Chemicals, Inc. (Boston, USA). The content of boron was approximately 2.5 wt% as introduced and the sodium concentration was ~ 0.72 wt% as detected. Commercial colloidal silica (LUDOX[®] LS) with the original pH value of 8.2 was obtained from Sigma-Aldrich (St Louis, USA). The SiO_2 content was 30 wt%. PVP ($M_w = 1,300,000$) was provided by Bodi Chemical Co., Ltd. (Tianjin, China). Absolute ethanol was purchased from Hengxing Chemical Reagent Co., Ltd. (Tianjin, China). All chemicals were used as received. Deionized water was prepared in the laboratory.

Synthesis of diphasic mullite nanofibers

Aluminum acetate was added into deionized water to acquire a 20 wt% aqueous solution and stirred at 40 °C for 12 h to obtain alumina sol. By zeta potential analysis, the colloid particles in alumina sol got positive charge. However, the surface of silica particles in commercial colloidal silica is charged with negative electricity. To avoid generating precipitation when mixing the two sols, dilute nitric acid (1 wt%) was added into colloidal silica to make the silica particle surface carry positive charge by adjusting the pH from 8.2 to 4.3. The molar ratio of Al_2O_3 : SiO_2 : B_2O_3 was designed to be 3:2:1. Alumina sol and acidulated colloidal silica were mixed together to acquire the mullite precursor sol. All sol products were colorless and transparent. PVP was dissolved into alcohol with a concentration of 16 wt% to prepare PVP solution. To obtain a spinning solution that is suitable for electrospinning and able to prepare uniform nanofibers, PVP solution and precursor sol were mixed with the mass ratios of 0.75, 1.0, 1.5 and 2.5, respectively. After stirring for 1 h at room temperature, homogeneous spinning solutions were obtained. Afterward, each spinning solution was

transferred into a plastic syringe equipped with a metallic needle. The needle was connected to a negative voltage supply. Electrospinning was carried out using a voltage of -6.45 kV, a feeding rate of 0.2 ml h^{-1} and a distance of 15 cm between the needle tip and the grounded collector. As-spun precursor nanofibers were dried at 40 °C for 5 h to remove the residual solvent for morphology investigation. The optimal fibers were heated to 800 °C in air circumstance with a heating rate of 5 °C min^{-1} and kept for 1 h. After that, the samples were calcined from 800 to 1200 °C for an extra 1 h.

Characterization

The conductivity of the spinning solutions was measured by a DDS-11A digital conductivity meter (Leici, China) at 25 °C.

The morphology of the nanofibers was examined by a Quanta FEG 250 (FEI, USA) scanning electron microscope (SEM). The image analysis software Image J was used to calculate the diameters of the nanofibers. For each sample, 200 fibers were selected randomly for measurement to acquire accurate data. The chemical structures of the precursor gel, PVP and as-spun nanofibers were investigated by Fourier transform infrared (FT-IR) absorption spectra measured by a Model 6700 spectrometer (Nicolet, USA) using the KBr pellet method. All samples were ground to powders for FT-IR analyses. Thermal analyses (TG–DSC) of the as-spun precursor nanofibers were performed on a STA-449C thermoanalyzer (Netzsch, German) in air atmosphere at a heating rate of 10 °C min^{-1} with an end temperature of 1280 °C. The X-ray powder diffraction (XRD) data of the calcined samples were recorded by a D500 diffractometer (SIEMENS, German) using $\text{CuK}\alpha$ in the region of $10 < 2\theta < 80^\circ$. Diffraction peaks were indexed with Jade 6.0 software. The morphology of crystal grains was observed by a JEM-2100F (JEOL, Japan) transmission electron microscope (TEM). The elemental analyses of calcined nanofibers were examined by a Titan G2 60-300 (FEI, USA) transmission electron microscope equipped with an energy-dispersive X-ray spectroscopy (EDS). The elastic modulus of a single nanofiber was measured by a Multimode 8 atomic force microscope (AFM; Veeco, USA) using the three-point bending method under the force mode. The samples were prepared by depositing the as-calcined nanofibers on a silicon

wafer. The wafer had many 4- μm -wide etched grooves. The nanofiber deposited across the grooves was tested. The spring constant and deflection sensitivity of the cantilever were 155.11 N m^{-1} and 35.622 nN V^{-1} , respectively. The modulus value was calculated according to the following formula [22, 23]:

$$E = \frac{FL^3}{192\delta I}$$

where F is the applied force, L is the suspended length, δ is the deflection of the beam at midspan and I is the second moment of area of the beam (where $I = \pi D^4/64$ and D is the fiber diameter). Five readings were taken from the measured fiber to obtain the modulus value.

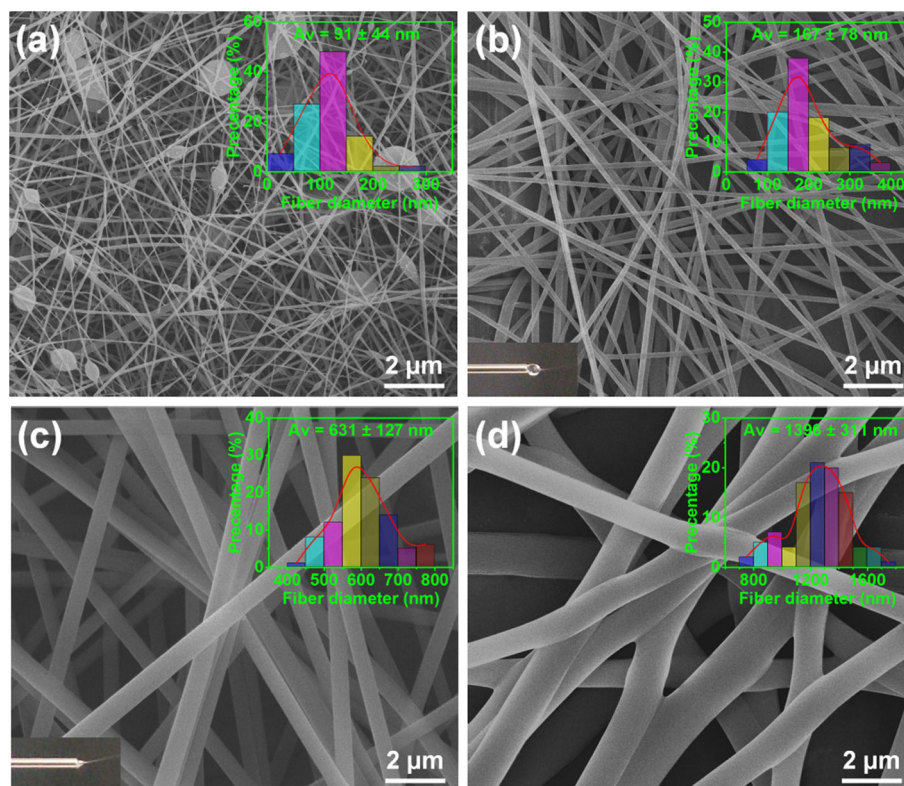
Results and discussion

Morphology and chemical structure of as-spun nanofibers

The SEM images and diameter distribution histograms of the as-spun precursor nanofibers prepared from spinning solutions with different mass

ratios of PVP solution to precursor sol are displayed in Fig. 1. All samples showed the fiber-like structure, revealing that electrospinning the solutions prepared using diphasic mullite sol was feasible. Besides, it was evident that the diameters increased with the increased mass ratio of PVP solution to precursor sol. These results could be explained by the rheological properties and conductivity of the spinning solutions as shown in Fig. 2. It was credible that continuous electrospun fibers were formed since all the four solutions showed shear thinning behavior [20]. Moreover, the increased viscosity and decreased conductivity of the spinning solutions were the main reasons that led to the increase in fiber diameters [24]. When the mass ratio of PVP solution to precursor sol was 0.75, Fig. 1a showed that the fibers with an average diameter of 91 nm were disconnected and lots of beads generated. When the mass ratio increased to 1.0 (Fig. 1b), average fiber diameter increased to 167 nm. Though the fibers owned straight and continuous structure, the electrospinning process did not run continuously. As observed in the bottom in Fig. 1b, a liquid bead, which was affirmed to be the precursor sol, appeared on the needle tip after electrospinning for 3 min and would drop down within limited time. During the entire electrospinning

Figure 1 SEM images of as-spun precursor nanofibers prepared using different mass ratios of PVP solution to precursor sol: **a** 0.75, **b** 1.0, **c** 1.5 and **d** 2.5; the top insets show the diameter distribution histograms and the bottom insets show the needle appearance after electrospinning for 3 min.



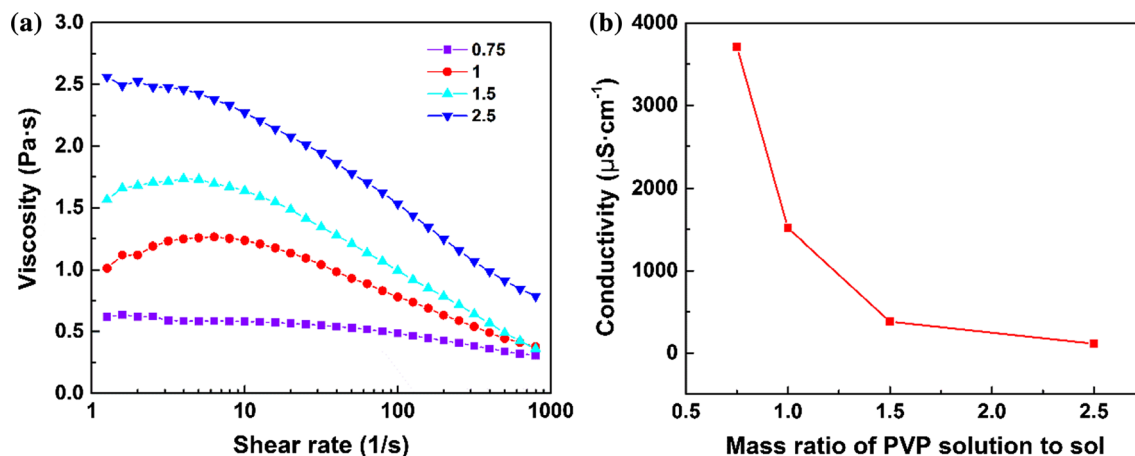


Figure 2 a Rheological properties and b conductivity of spinning solutions prepared with different mass ratios of PVP solution to precursor sol.

process, lots of liquid beads dropped, which meant that a certain amount of precursor sol could not be carried by PVP to form the fiber-like structure since the PVP content was too low. While at the mass ratio of 1.5 (Fig. 1c), straight and continuous nanofibers with smooth surface and cylindrical structure were obtained. Such fibers had diameters ranging from 400 to 800 nm and an average diameter of 631 nm. As revealed in the bottom in Fig. 1c, no liquid bead appeared on the needle tip any more during the entire electrospinning process, indicating the stable spinning performance. When the mass ratio was 2.5 (Fig. 1d), the joints of the as-spun nanofibers bonded together mostly. This was because that the solvent in the as-spun nanofibers did not evaporate completely during the electrospinning process due to the large fiber diameters (1396 nm). Based on the above analyses, the proper mass ratio of PVP solution to precursor sol in the present work was 1.5.

The miscibility between precursor sol and polymer additive had significant effects on the morphology of electrospun ceramic nanofibers [25, 26]. Generally, when smooth as-spun fibers undergone calcination, good miscibility led to smooth surface while bad miscibility resulted in rough feature. Therefore, the miscibility between the diphasic mullite sol and PVP solution was discussed. Previous research proposed that the alumina sol, which was prepared using the same aluminum source, mixed well with PVP solution [24]. But the colloidal silica might not because of the interaction of silica colloidal particles with PVP [27]. The appearance of the mixture of acidulated colloidal silica and PVP solution and the spinning

solution is shown in Fig. 3. The mass ratios of acidulated colloidal silica to PVP for the two samples were same. As observed, the former mixture was gray-white and opaque, indicated that the miscibility between colloidal silica and PVP solution was not good. However, the spinning solution was transparent. This might be due to that the interfacial properties of the colloidal particles of silica changed by mixing with alumina sol, which improved the miscibility with PVP solution consequently. Even so, it could still not be concluded that the immiscibility between PVP solution and colloidal silica had vanished at this point.

The chemical structure of diphasic mullite gel, PVP and as-spun nanofibers is investigated. Figure 4 displays the corresponding FT-IR spectra in the 2000–400 cm^{-1} range. For as-spun nanofibers, the

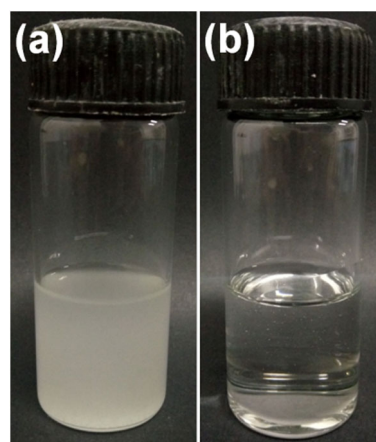


Figure 3 Optical photographs of a mixed solution of acidulated colloidal silica and PVP solution and b spinning solution.

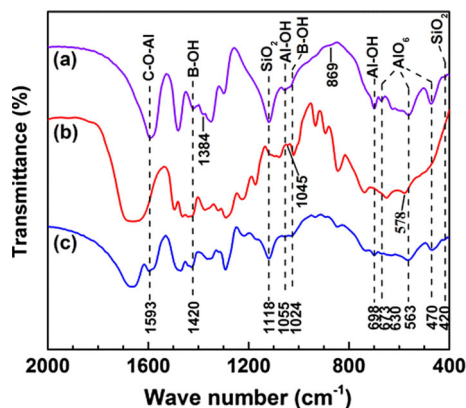


Figure 4 FT-IR spectra of **a** diphasic mullite gel, **b** PVP and **c** as-spun nanofibers.

majority of the characteristic peaks of precursor gel and PVP retained. The peaks at 1420 and 1024 cm^{-1} were due to the B–OH bend in boric acid introduced by aluminum acetate [28]. The band at 1593 cm^{-1} could be ascribed to the C–O bonding with Al in $\text{Al}(\text{OH})_2(\text{OOCCH}_3)$ [29]. The peaks at 1118 and 420 cm^{-1} were corresponded to the Si–O–Si group in SiO_2 [30, 31] while the peaks located in 1055 and 698 cm^{-1} were assigned to the Al–OH bend from precursor gel [31, 32]. In addition, the bands observed at 673, 563 and 470 cm^{-1} were attributed to the Al–O stretch in AlO_6 normally [32–34]. Other peaks were basically due to the characteristic groups of CH_2 , C–H, C–C, C–N and N–C=O in PVP [35]. However, some weak peaks of precursor gel were covered by the adjacent strong peaks of PVP after mixing the precursor sol and PVP solution, and vice versa. For example, the peaks at 1384 and 869 cm^{-1} corresponding to the N=O symmetric stretching vibration in NO_3^- [30, 31] and the Al–O stretching vibration in AlO_4 [32] appeared in gel could not be observed in as-spun fibers. Besides, the bands at 1045 and 578 cm^{-1} assigned to bonds of C–O–C and N–C=O [35] which existed in PVP vanished either. These analyses revealed that no chemical reaction took place while preparing the spinning solution and as-spun nanofibers despite the immiscibility between colloidal silica and PVP solution.

Microstructure evolution of diphasic mullite nanofibers during calcination

Heat treatment

The thermal behavior of as-spun composite nanofibers is shown in Fig. 5. Three major mass losses during the heating process could be observed from the TG curve. The mass loss of 5.5 wt% below 160 °C was caused by the removal of absorbed water. The corresponding endothermic peak was evident at 89 °C in the DSC curve. While from 160 to 396 °C, a significant mass loss of about 40 wt% was observed. This was associated with two endothermic peaks at 228 and 301 °C and one exothermic peak at 389 °C in the DSC curve, which was induced by the decomposition of boric acid and organic groups existed in the precursor gels and the thermal oxidative degradation of PVP. The third mass loss of 24.6 wt% between 396 and 1000 °C was caused by the decomposition of residual organic groups and PVP, and the elimination of the decomposition gaseous products such as CO_2 , H_2O . The exothermic peak at 507 °C was attributed to these reactions. When calcination temperature reached to 1200 °C, a ceramic yield of 29.9% was obtained. Additionally, an exothermic peak emerged at 893 °C. To pure diphasic mullite, alumina in gamma form usually generates first. However, due to the presence of B_2O_3 , amorphous Al_2O_3 will react with B_2O_3 to form $\text{Al}_4\text{B}_2\text{O}_9$ phase generally [36, 37]. Considering the introduced boron content, the peak was assigned to the formation of $\text{Al}_4\text{B}_2\text{O}_9$ phase. As we know, $\text{Al}_4\text{B}_2\text{O}_9$ would transform to $\text{Al}_{18}\text{B}_4\text{O}_{33}$ and mullite would form with temperature increased [36, 37], but no exothermic peak corresponded to the two reactions was found.

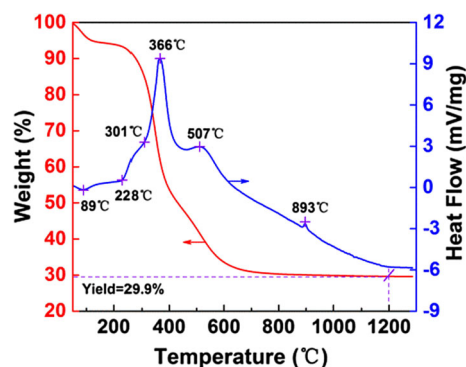


Figure 5 TG–DSC curves of as-spun nanofibers at a heating rate of 10 °C min^{-1} .

Phase transformation

Figure 6 shows the XRD patterns of the ceramic nanofibers calcined at 800, 1000 and 1200 °C. As observed, no distinct diffraction peak appeared at 800 °C, implying that no phase formed at this temperature. A distinct broad hump appeared between the 2θ of about 12° and 38° was attributed to the presence of amorphous SiO₂. When the temperature reached up to 1000 °C, Al₄B₂O₉ phase was detected and this was in consistent with the DSC analyses. The hump assigned to amorphous SiO₂ could also be observed. While for the sample calcined at 1200 °C, four additional diffraction peaks with low intensity at the 2θ of 20.3°, 23.7°, 48.5° and 75.1° were observed, indicating that Al₄B₂O₉ phase had transformed to Al₁₈B₄O₃₃ phase. Besides, the intensities of the two diffraction peaks located at the 2θ of 16.5 and 26.2° reversed. This was a significant evidence to verify that mullite phase had formed in Al₂O₃–SiO₂–B₂O₃ ternary ceramics [38]. Since mullite phase formed, amorphous SiO₂ decreased in content, but it still existed.

From these analyses, the phase evolution of the boron-containing diphasic mullite nanofibers in the present work could be summarized as follows:

Amorphous → Al₄B₂O₉ + amorphous SiO₂ → Al₁₈B₄O₃₃ + mullite + amorphous SiO₂.

Such process was same with the typical phase transformation route of pure diphasic mullite products from amorphous state to mullite phase after replacing alumina borate phases by γ -Al₂O₃ [13]. SiO₂

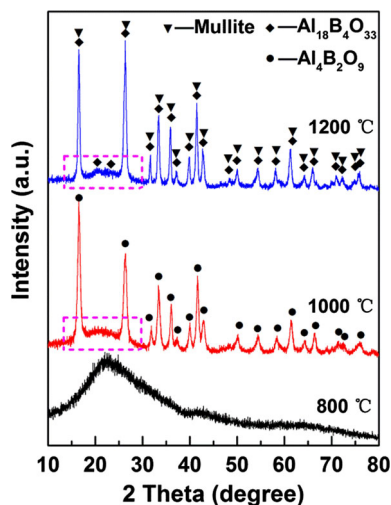


Figure 6 XRD patterns of mullite nanofibers calcined at different temperatures.

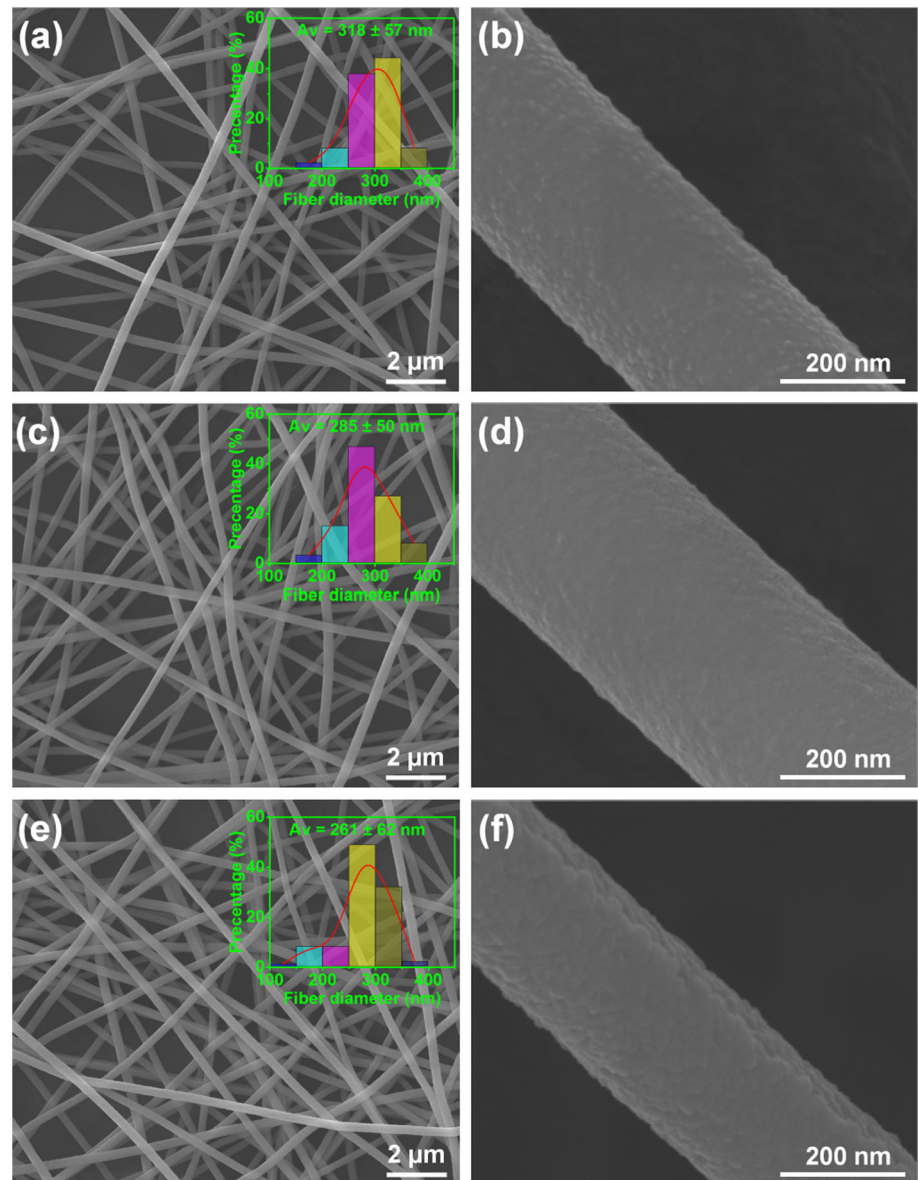
in amorphous state was benefit for the diphasic mullite nanofibers to acquire preferable flexibility under deformation and keep stable structure at high temperatures.

Morphology evolution

SEM images and diameter distribution histograms of mullite nanofibers obtained at 800, 1000 and 1200 °C are displayed in Fig. 7. It could be observed from Fig. 7a, c, e that all fiber samples kept straight, continuous and uniform structure after calcining at elevated temperatures. But the calculated average diameters were different. For the sample prepared at 800 °C, the average diameter was 318 nm. This was much smaller than that of the as-spun nanofibers because of the removal of PVP and other organics. When temperature increased to 1000 °C, the average diameter decreased to 285 nm. XRD results showed that Al₄B₂O₉ formed at this temperature. Thus, the densification took place and the average fiber diameter decreased. In addition, owing to the formation of the viscous flow of amorphous phase, the closure of tiny voids or cracks occurred and the dispersive grains became compact. The densification process was promoted then, which contributed to the diameter decrease. After calcining at 1200 °C, the average diameter decreased to 261 nm. Though the content of amorphous SiO₂ reduced due to the formation of mullite, the densification process still proceeded.

Beyond that, distinct microscopic differences were found from the high-magnification SEM images (Fig. 7b, d, f). The fiber surface was rough after calcining at 800 °C, but it became relatively smooth at 1000 °C, and the surface turned back to rough again at 1200 °C. This was a novel rule for surface evolution while preparing electrospun mullite nanofibers at elevated temperatures. The schematic diagram of possible formation mechanism for the different surface morphology at different temperatures is illustrated in Fig. 8a. TEM images of mullite nanofibers obtained at 800, 1000 and 1200 °C are displayed in Fig. 8b, c, d to verify the inferences. Since XRD results showed that no crystal phase formed at 800 °C, the surface particles should not be regarded as crystalline grains, but amorphous Al₂O₃, B₂O₃ and SiO₂ particles. This conclusion is confirmed by Fig. 8b. From the rough surface feature, it could be concluded that the immiscibility between colloidal silica and PVP solution did not vanish and the phase separation of

Figure 7 SEM images of mullite nanofibers obtained at **a, b** 800 °C, **c, d** 1000 °C and **e, f** 1200 °C, the insets show the diameter distribution histograms.

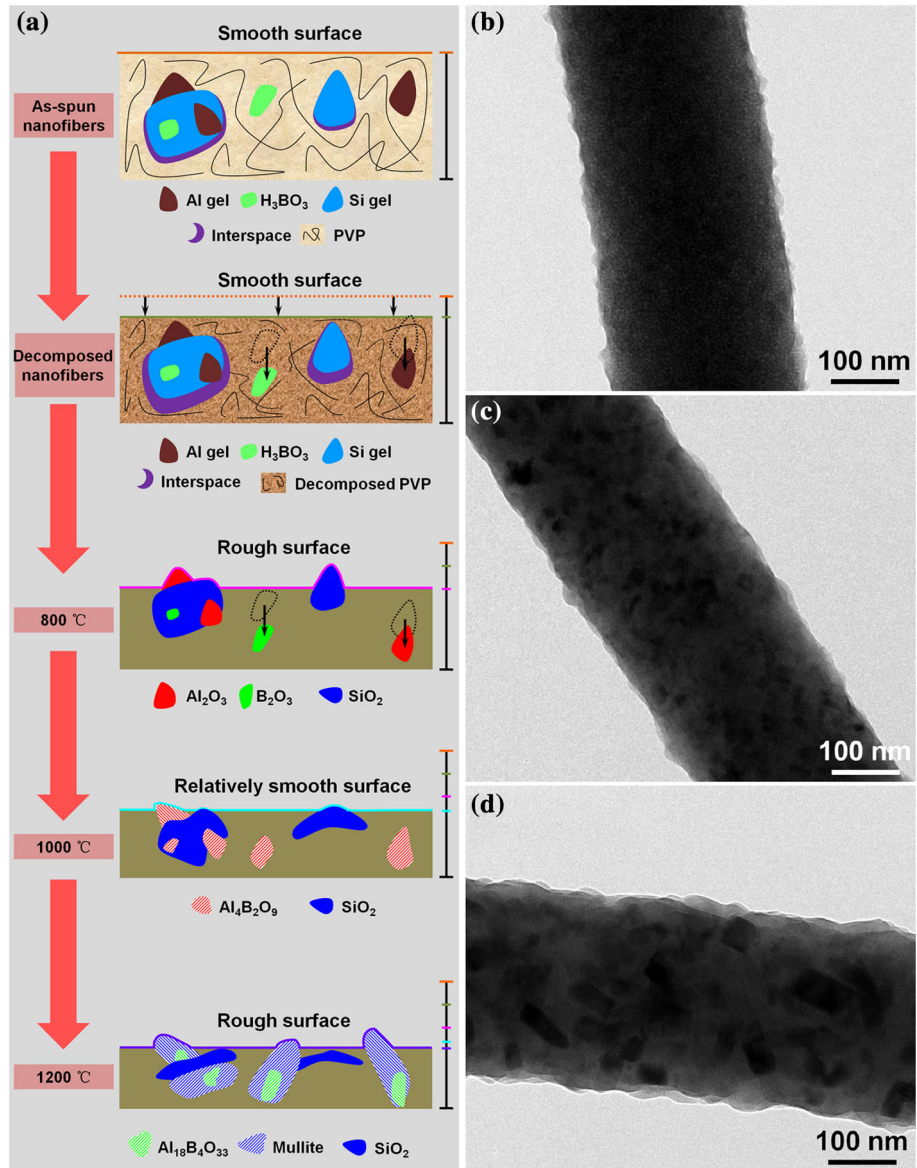


precursor gel and PVP in as-spun nanofibers occurred. As shown in Fig. 8a, many interspaces between silica gel and PVP emerged due to the phase separation. During the decomposition process, independent particles of alumina gel and boric acid moved to the fiber axes. However, the motions of silica gel and composite gel were hindered by the interspaces. When PVP and other organics decomposed completely, rough fiber surface was obtained.

For nanofibers calcined at 1000 °C, the reasons for the relatively smooth surface could be deduced easily according to the discussions about the decrease in fiber diameters. On the one hand, as seen in Fig. 8a, some raised amorphous particles melted to transform

to the viscous flow state, which was benefit to improve the smooth degree. On the other hand, some unmelted particles on the surface might move into the fiber inner due to the motion of the viscous flow [39, 40]. Therefore, the rough degree reduced significantly. It could be concluded that the diphasic gel-derived electrospun mullite nanofibers possessed self-repairing ability for surface defects owing to the viscous flow generated from the amorphous phase. However, there were still some small promontories on the surface. It was believed that they were inherited from the imperfect morphology obtained at 800 °C, instead of generating by grain growth. Such deduction is verified by the observation of grains

Figure 8 a Schematic diagrams of possible evolution mechanism for surface evolution and TEM images of mullite nanofibers obtained at b 800 °C, c 1000 °C and d 1200 °C.



shown in Fig. 8c. As observed, some large grains did not grow to the surface layer, and those located at the surface layer were normally small.

After calcining at 1200 °C, $\text{Al}_4\text{B}_2\text{O}_9$ had transformed to $\text{Al}_{18}\text{B}_4\text{O}_{33}$ and mullite had formed. As reported, alumina borate could act as epitaxial substrates for mullite nucleation and growth [41]. Mullite could grow directly on alumina borate grains along an assigned crystal orientation. As a consequence, large and elongated crystal grains were generated (Fig. 8d), and this was the main reason for the rough fiber surface.

Elemental analyses and mechanical properties of mullite nanofibers

Elemental distribution and chemical composition

Considering the ideal morphology, the elemental distribution and chemical composition of mullite nanofibers obtained at 1000 °C were detected. Figure 9 exhibits the HAADF STEM image, elemental mappings and EDS spectrum of a single mullite nanofiber. Table 1 lists the chemical composition derived from EDS. As displayed in Fig. 9a, the center axis portions of the fiber were much lighter than the two edges. This apparent contrast indicated that the sample was thicker in the axes than at the edges,

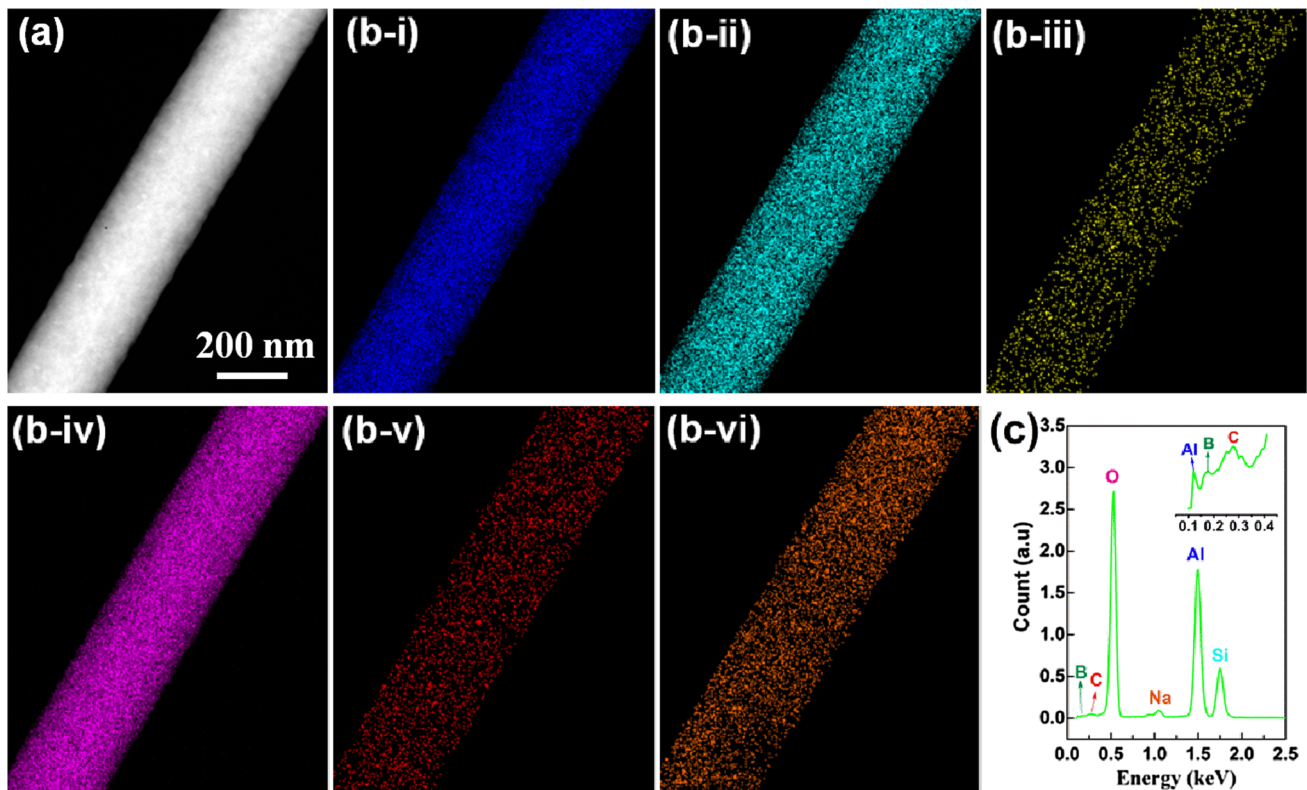


Figure 9 a HAADF STEM image, b elemental mappings of (i) Al, (ii) Si, (iii) B, (iv) O, (v) C and (vi) Na, and c EDS spectrum of mullite nanofibers calcined at 1000 °C.

Table 1 Chemical composition of mullite nanofibers derived from EDS spectrum

Elements	Al	Si	B	O	C	Na	Al/Si
Wt (%)	33.96	11.87	2.79	48.80	1.28	1.30	
At (%)	24.42	8.20	5.00	59.19	2.07	1.10	2.98

which verified the cylindrical structure of the nanofibers. The elemental mappings presented in Fig. 9b demonstrated that Al, Si, B, O, C and Na were all uniformly distributed, revealing the homogeneous feature of the prepared nanofibers. Such result also demonstrated that no segregation of any element emerged though the miscibility between colloidal silica and PVP solution was not good and the phase separation of precursor gel and PVP occurred. And it could also be concluded that the densification process during calcination proceeded uniformly.

The EDS spectrum verified the presence of these elements (Fig. 9c). Table 1 showed that the detected molar ratio of Al to Si was 2.98, which was basically

equal to the designed value (3.0, same with that of pure mullite). However, the content of boron was lower than the stoichiometric amount (4.3 wt%). The experimental error was an important reason for this because B could not be detected accurately by EDS method. In addition, Stachewicz et al. [42] had reported that surface elements of electrospun nanofibers prepared using different electrostatic polarities were different due to the different electrostatic forces acted on the atoms. Since EDS only provided exact element compositions of the fiber surface within depth of 5–10 nm, one possible explanation for the low content was that boron might run to the core of the nanofibers during electrospinning. Beyond that, Na was introduced by the raw materials and C was caused by the incomplete decomposition of PVP and acetate. Undoubtedly, the incoming Na and the residual C had significant effects on mechanical properties and high-temperature structural stability of the mullite nanofibers. Therefore, purifying the colloidal silica before using and removing the total carbon during calcination would be important issues for further study.

Elastic modulus and flexibility

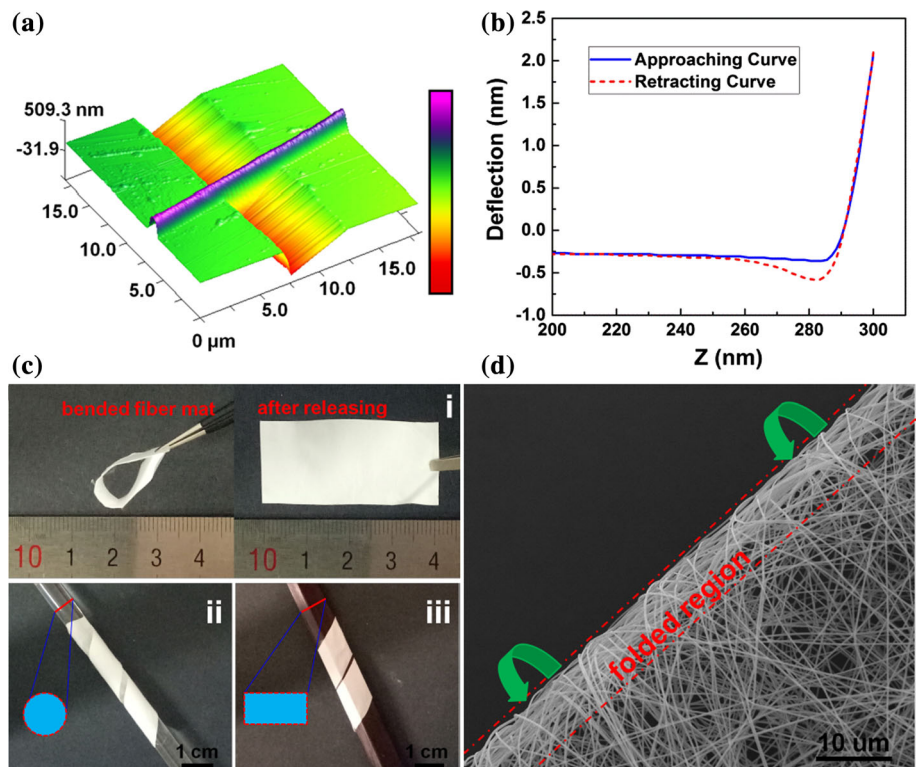
The room temperature elastic modulus of the mullite nanofibers obtained at different temperatures was measured. Figure 10a shows the 3D AFM image of a single nanofiber suspended over a groove on silicon wafer. The fiber attached closely to the wafer surface and deposited across the groove, suggesting the desired beam structure for three-point bending method. Figure 10b exhibits an intact force curve composed of an approaching part and a retracting part obtained by AFM. The approaching curve was used to calculate the elastic modulus. The diameter of the fiber was determined from the height profile of the beam structure. The diameters and calculated modulus values of the nanofibers are listed in Table 2. As could be seen, the elastic modulus increased from 16.76 ± 1.52 to 25.18 ± 1.29 GPa with the calcination temperatures increased from 800 to 1000 °C. This was mainly caused by the formation of $Al_4B_2O_9$ phase. The modulus value reached to 37.45 ± 2.07 GPa for sample prepared at 1200 °C. The increased grain sizes, phase transformation and decreased amount of amorphous phase were ascribed to this [43]. Obviously, the modulus values were much lower than that of Nextel™ 312 fibers (152

Table 2 Elastic modulus of mullite nanofibers obtained at different temperatures

Temperature (°C)	Diameter (nm)	Elastic modulus (GPa)
800	307	16.76 ± 1.52
1000	295	25.18 ± 1.29
1200	311	37.45 ± 2.07

GPa) [3]. For mullite fiber products, the lower elastic modulus indicated the better flexibility. The sample prepared at 1000 °C was tested to show its flexibility. As observed in Fig. 10c, the fiber mat could be bended to a small radius and retain continuous after releasing. Moreover, it could also be wrapped on a cylindrical glass rod and a quadrangle rod tightly without any fracture. In Fig. 10d, details of the folded fiber mat showed that even no breakage emerged in the folded region. Such results revealed the outstanding flexibility of the mullite nanofibers. Owing to the flexible feature, the diphasic mullite nanofibers show potential application within the thermal insulation area. They are also promising to be used as the starting materials to prepare mullite nanofiber-based sponges, aerogels or composites for industrial

Figure 10 a 3D AFM image of a single mullite nanofiber suspended over a groove, b a representative force curve obtained by AFM, c optical photographs showing the outstanding flexibility, and d SEM image of the folded nanofiber mat.



application, or used as catalyst carriers, adsorbing materials or filter materials.

Conclusions

Homogeneous and flexible mullite nanofibers derived from conventional diphasic mullite sol were successfully prepared by electrospinning technique for the first time. When the mass ratio of PVP solution to precursor sol was 1.5, the electrospinning performance and the morphology of the as-spun nanofibers were preferable. No chemical reaction took place during the process of preparing spinning solution and electrospinning though the miscibility between colloidal silica and PVP solution was not good. Upon heating under air circumstance, a ceramic yield of 29.9% at 1200 °C was obtained. $\text{Al}_4\text{B}_2\text{O}_9$ and $\text{Al}_{18}\text{B}_4\text{O}_{33}$ phase formed due to the reaction between Al_2O_3 and B_2O_3 . After calcining at 1200 °C, mullite phase was detected. With the calcination temperature increased from 800 to 1200 °C, the average fiber diameter decreased from 318 to 261 nm unceasingly because the densification occurred. Rough fiber surface emerged at 800 °C because of the phase separation of precursor gel and PVP. The surface turned to be relatively smooth at 1000 °C owing to the viscous flow of amorphous SiO_2 , and be rough again at 1200 °C due to the grain growth. For mullite nanofibers obtained at 1000 °C, the Al/Si molar ratio was 2.98 and all elements distributed uniformly, showing the homogeneous feature. The low elastic modulus of 25.18 ± 1.29 GPa and the good bended and folded features revealed the outstanding flexibility.

Acknowledgements

The authors gratefully acknowledge the financial support from the “Chang Jiang Scholars Program” of the Ministry of Education of China (Grant No. T2011119).

Compliance with ethical standards

Conflict of interest The authors declared that they have no conflict of interest.

References

- [1] Wang Y, Cheng H, Liu H, Wang J (2013) Microstructure and room temperature mechanical properties of mullite fibers after heat-treatment at elevated temperatures. *Mater Sci Eng A* 578:287–293
- [2] Schawaller D, Clauß B, Buchmeiser MR (2012) Ceramic filament fibers—a review. *Macromol Mater Eng* 297:502–522
- [3] Bunsell AR, Berger MH (2000) Fine diameter ceramic fibres. *J Eur Ceram Soc* 20:2249–2260
- [4] Dong X, Sui G, Guo A et al (2015) Synthesis and properties of lightweight flexible insulant composites with a mullite fiber-based hierarchical heterostructure. *Chem Eng J* 277:159–167
- [5] Wilson DM, Visser LR (2001) High performance oxide fibers for metal and ceramic composites. *Compos Part A Appl Sci Manuf* 32:1143–1153
- [6] Koch D, Tushtev K, Grathwohl G (2008) Ceramic fiber composites: experimental analysis and modeling of mechanical properties. *Compos Sci Technol* 68:1165–1172
- [7] Si Y, Yu J, Tang X et al (2014) Ultralight nanofibre-assembled cellular aerogels with superelasticity and multifunctionality. *Nat Commun* 5:1–9
- [8] Wang H, Zhang X, Wang N et al (2017) Ultralight, scalable, and high-temperature-resilient ceramic nanofiber sponges. *Sci Adv* 3:1–10
- [9] Wu H, Pan W, Lin D, Li H (2012) Electrospinning of ceramic nanofibers: fabrication, assembly and applications. *J Adv Ceram* 1:2–23
- [10] Wu J, Lin H, Li J-B et al (2009) Fabrication and characterization of electrospun mullite nanofibers. *Mater Lett* 63:2309–2312
- [11] Mohammad Ali Zadeh M, Keyanpour-Rad M, Ebadzadeh T (2014) Effect of viscosity of polyvinyl alcohol solution on morphology of the electrospun mullite nanofibres. *Ceram Int* 40:5461–5466
- [12] Peng C, Liu P, Hu J et al (2014) Preparation of uniaxially aligned mullite ceramic fibers by electrospinning. *Colloids Surf A Physicochem Eng Asp* 457:1–7
- [13] Cividanes LS, Campos TMB, Rodrigues LA et al (2010) Review of mullite synthesis routes by sol–gel method. *J Sol–Gel Sci Technol* 55:111–125
- [14] Sowman HG (1974) Aluminum borate and aluminum borosilicate articles. U.S. Patent 3,795,524
- [15] Schmücker M, Flucht F, Schneider H (1996) High temperature behaviour of polycrystalline aluminosilicate fibres with mullite bulk composition. I. Microstructure and strength properties. *J Eur Ceram Soc* 16:281–285

- [16] Mohammad Ali Zadeh M, Keyanpour-Rad M, Ebadzadeh T (2013) Synthesis of mullite nanofibres by electrospinning of solutions containing different proportions of polyvinyl butyral. *Ceram Int* 39:9079–9084
- [17] Wu J, Lin H, Li J et al (2010) Synthesis and characterization of electrospun mullite nanofibers. *Adv Eng Mater* 12:71–74
- [18] Zhou J, Sun G, Zhao H et al (2015) Tunable white light emission by variation of composition and defects of electrospun Al_2O_3 - SiO_2 nanofibers. *Beilstein J Nanotechnol* 6:313–320
- [19] Wei H, Li H, Cui Y et al (2017) Synthesis of flexible mullite nanofibres by electrospinning based on nonhydrolytic sol-gel method. *J Sol-Gel Sci Technol* 82:718–727
- [20] Dong X, Liu J, Li X et al (2017) Electrospun mullite nanofibers derived from diphasic mullite sol. *J Am Ceram Soc* 100:3425–3433
- [21] Richards EA, Goodbrake CJ, Sowman HG (1991) Reactions and microstructure development in mullite fibers. *J Am Ceram Soc* 74:2404–2409
- [22] Tan EPS, Lim CT (2006) Effects of annealing on the structural and mechanical properties of electrospun polymeric nanofibres. *Nanotechnology* 17:2649–2654
- [23] Ding Y, Zhang P, Jiang Y et al (2009) Mechanical properties of nylon-6/ SiO_2 nanofibers prepared by electrospinning. *Mater Lett* 63:34–36
- [24] Song X, Liu W, Wang J et al (2017) Microstructural differences between electrospun alumina borate nanofibers prepared by solutions with different PVP contents. *Ceram Int* 43:9831–9837
- [25] Dai Y, Liu W, Formo E et al (2011) Ceramic nanofibers fabricated by electrospinning and their applications in catalysis, environmental science, and energy technology. *Polym Adv Technol* 22:326–338
- [26] Liu P, Zhu Y, Ma J et al (2013) Preparation of continuous porous alumina nanofibers with hollow structure by single capillary electrospinning. *Colloids Surf A Physicochem Eng Asp* 436:489–494
- [27] Zeng L, Weber AP (2014) Aerosol synthesis of nanoporous silica particles with controlled pore size distribution. *J Aerosol Sci* 76:1–12
- [28] Zhihong L, Shiyang G, Shuping X (2003) FT-IR spectroscopic study of phase transformation of chloropinoite in boric acid solution at 303 K. *Spectrochim Acta Part A Mol Biomol Spectrosc* 59:265–270
- [29] Fu Q, Cao CB, Zhu HS (1999) Preparation of alumina films from a new sol-gel route. *Thin Solid Films* 348:99–102
- [30] Zhang Y, Ding Y, Gao J, Yang J (2009) Mullite fibres prepared by sol-gel method using polyvinyl butyral. *J Eur Ceram Soc* 29:1101–1107
- [31] Leivo J, Lindén M, Rosenholm JM et al (2008) Evolution of aluminosilicate structure and mullite crystallization from homogeneous nanoparticulate sol-gel precursor with organic additives. *J Eur Ceram Soc* 28:1749–1762
- [32] Beran A, Voll D, Schneider H (2001) Dehydration and structural development of mullite precursors: an FTIR spectroscopic study. *J Eur Ceram Soc* 21:2479–2485
- [33] Ksapabutr B, Gulari E, Wongkasemjit S (2004) Sol-gel transition study and pyrolysis of alumina-based gels prepared from alumatrane precursor. *Colloids Surf A Physicochem Eng Asp* 233:145–153
- [34] Jing C, Zhao X, Zhang Y (2007) Sol-gel fabrication of compact, crack-free alumina film. *Mater Res Bull* 42:600–608
- [35] Borodko Y, Habas SE, Koebel M et al (2006) Probing the interaction of poly(vinylpyrrolidone) with platinum nanocrystals by UV-Raman and FTIR. *J Phys Chem B* 110:23052–23059
- [36] Lührs H, Fischer RX, Schneider H (2012) Boron mullite: formation and basic characterization. *Mater Res Bull* 47:4031–4042
- [37] Zhang G, Fu Z, Wang Y et al (2010) Boron-doped mullite derived from single-phase gels. *J Eur Ceram Soc* 30:2435–2441
- [38] Sowman HG (1988) Alumina-boria-silica ceramic fibers from the sol-gel process. In: Klein LC (ed) *Sol-gel technology for thin films, fibers, performs, electronics, and specialty shapes*. Noyes Publications, Park Ridge, pp 162–182
- [39] Saruhan B, Albers W, Schneider H, Kaysser WA (1996) Reaction and sintering mechanisms of mullite in the systems cristobalite/ α - Al_2O_3 and amorphous SiO_2 / α - Al_2O_3 . *J Eur Ceram Soc* 16:1075–1081
- [40] Salomão R, Fernandes L (2017) Porous co-continuous mullite structures obtained from sintered aluminum hydroxide and synthetic amorphous silica. *J Eur Ceram Soc* 37:2849–2856
- [41] Hong SH, Cermignani W, Messing GL (1996) Anisotropic grain growth in seeded and B_2O_3 -doped diphasic mullite gels. *J Eur Ceram Soc* 16:133–141
- [42] Stachewicz U, Stone CA, Willis R, Barber AH (2012) Charge assisted tailoring of chemical functionality at electrospun nanofiber surfaces. *J Mater Chem* 22:22935–22941
- [43] Song X, Liu W, Xu S et al (2018) Microstructure and elastic modulus of electrospun Al_2O_3 - SiO_2 - B_2O_3 composite nanofibers with mullite-type structure prepared at elevated temperatures. *J Eur Ceram Soc* 38:201–210